

IEEE

GEOSCIENCE AND REMOTE SENSING LETTERS

A PUBLICATION OF THE IEEE GEOSCIENCE AND REMOTE SENSING SOCIETY



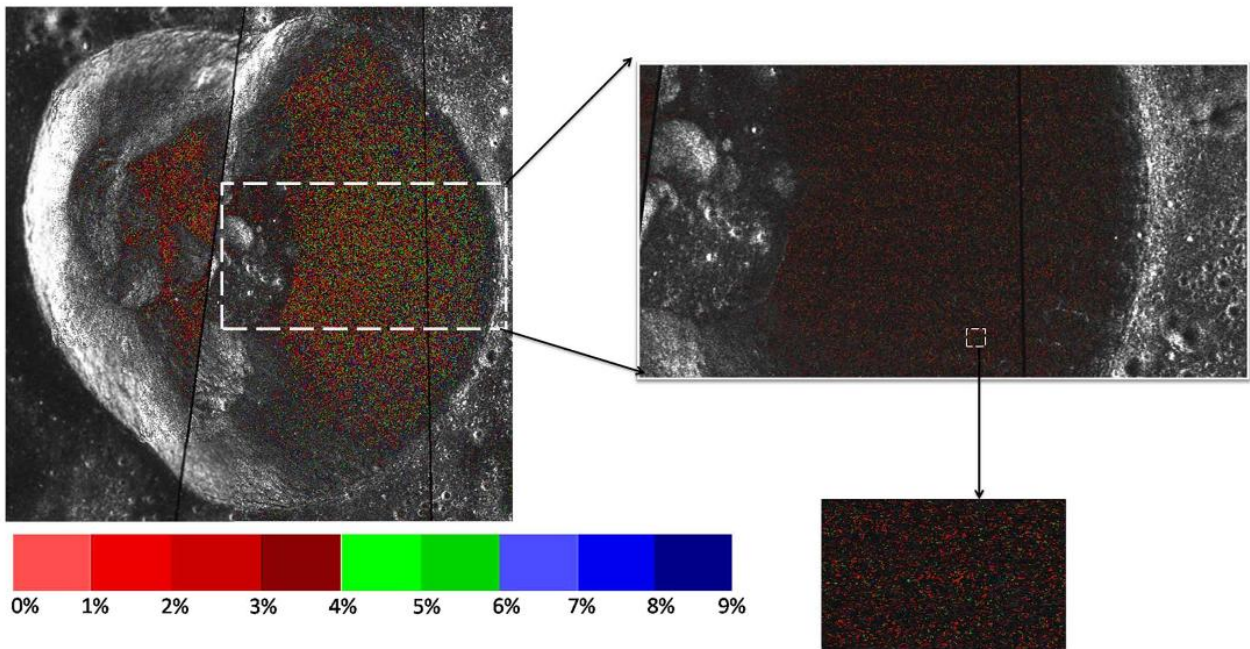
JULY 2016

VOLUME 13

NUMBER 7

IGRSBY

(ISSN 1545-598X)



Estimation of percentage of water ice within Hermite-A crater over the Lunar North Pole using Mini-RF datasets.

IEEE

GEOSCIENCE AND REMOTE SENSING LETTERS

A PUBLICATION OF THE IEEE GEOSCIENCE AND REMOTE SENSING SOCIETY



JULY 2016

VOLUME 13

NUMBER 7

IGRSBY

(ISSN 1545-598X)

PAPERS

Oceans and Water

Cross-Correlation Between Polarization Channels in SAR Imagery Over Oceanographic Features
. *C. Brekke, C. E. Jones, S. Skrunes, B. Holt, M. Espeseth, and T. Eltoft* 997

Cryosphere

Quantification of Water Ice in the Hermite-A Crater of the Lunar North Pole
. *O. P. N. Calla, S. Mathur, and K. L. Gadri* 926

Vegetation and Land Surface

Uncertainty Estimation of Local-Scale Land Surface Temperature Products Over Urban Areas Using Monte Carlo Simulations
. *Z. Mitranka, G. Doxani, F. Del Frate, and N. Chrysoulakis* 917

High-Resolution Soil Moisture Retrieval With ASCAT
. *D. B. Lindell and D. G. Long* 972

Image Processing, Analysis, and Classification

Pan-Sharpening by Multilevel Interband Structure Modeling
. *X. Lu, J. Zhang, T. Li, and Y. Zhang* 892

An Algorithm to Extract More Accurate Slopes From DEMs
. *Z. Chen, Y. Chen, X. Chen, and T. Ma* 939

An Efficient Infrared Small Target Detection Method Based on Visual Contrast Mechanism
. *Y. Chen and Y. Xin* 962

One-Class Gaussian Process for Possibilistic Classification Using Imaging Spectroscopy
. *L. Kalantari, P. Gader, S. Graves, and S. A. Bohlman* 967

Region-Based Retrieval of Remote Sensing Images Using an Unsupervised Graph-Theoretic Approach
. *B. Chaudhuri, B. Demir, L. Bruzzone, and S. Chaudhuri* 987

Active Learning Methods for Efficient Hybrid Biophysical Variable Retrieval
. *J. Verrelst, S. Dethier, J. P. Rivera, J. Muñoz-Marí, G. Camps-Valls, and J. Moreno* 1012

Hyperspectral Data Processing

Tensor Decomposition and PCA Jointed Algorithm for Hyperspectral Image Denoising
. *S. Meng, L.-T. Huang, and W.-Q. Wang* 897

Band Weighting via Maximizing Interclass Distance for Hyperspectral Image Classification
. *C. Yan, X. Bai, P. Ren, L. Bai, W. Tang, and J. Zhou* 922

GBM-Based Unmixing of Hyperspectral Data Using Bound Projected Optimal Gradient Method
. *C. Li, Y. Ma, J. Huang, X. Mei, C. Liu, and J. Ma* 952

(Contents Continued on Page 886)



Hopfield Neural Network Approach for Supervised Nonlinear Spectral Unmixing	<i>J. Li, X. Li, B. Huang, and L. Zhao</i>	1002
Multimetric Active Learning for Classification of Remote Sensing Data	<i>Z. Zhang, E. Pasolli, H. L. Yang, and M. M. Crawford</i>	1007
Radar Systems		
Transient Interference Mitigation via Supervised Matrix Completion	<i>M. Li, Z. He, and W. Li</i>	907
Refraction Angle Approximation Algorithm for Wall Compensation in TWRI	<i>J. Liu, L. Kong, X. Yang, and Q. H. Liu</i>	943
Computationally Efficient Transient Interference Excision Method for Skywave Over-the-Horizon Radar	<i>Z. Liu, H. Su, Q. Hu, and Z. Cheng</i>	1017
Technical Aspects of 205 MHz VHF Mini Wind Profiler Radar for Tropospheric Probing	<i>T. K. Samson, A. Kottayil, M. M. G., B. B. B., R. V., R. Rebello, V. K., M. P., S. K. R., and M. K.</i>	1027
Synthetic Aperture Radar		
Two-Dimensional Spectrum for Circular Trace Scanning SAR Based on an Implicit Function	<i>Y. Liao, W.-Q. Wang, and Q. H. Liu</i>	887
Adaptive Laplacian Eigenmap-Based Dimension Reduction for Ocean Target Discrimination	<i>L. Shi, L. Zhang, L. Zhao, L. Zhang, P. Li, and D. Wu</i>	902
Higher Order Statistics for Texture Analysis and Physical Interpretation of Polarimetric SAR Data	<i>X. Deng and C. López-Martínez</i>	912
Unsupervised SAR Image Change Detection Based on SIFT Keypoints and Region Information	<i>Y. Wang, L. Du, and H. Dai</i>	931
Full-Wave Scattering and Imaging Characterization of Realistic Trees for FOPEN Sensing	<i>D. Liao and T. Dogaru</i>	957
Improved SNR Optimum Method in POLDINSAR Coherence Optimization	<i>B. Wu, L. Tong, Y. Chen, and L. He</i>	982
Improved Channel Error Calibration Algorithm for Azimuth Multichannel SAR Systems	<i>X. Guo, Y. Gao, K. Wang, and X. Liu</i>	1022
Sparsity-Driven Change Detection in Multitemporal SAR Images	<i>F. Nar, A. Özgür, and A. N. Saran</i>	1032
Lidar Systems		
Reflective Imaging Solved by the Radon Transform	<i>G. Rigaud, J.-B. Bellet, G. Berginc, I. Berechet, and S. Berechet</i>	936
A Novel Noise Filtering Model for Photon-Counting Laser Altimeter Data	<i>X. Wang, Z. Pan, and C. Glennie</i>	947
Excitation Wavelength Analysis of Laser-Induced Fluorescence LiDAR for Identifying Plant Species	<i>J. Yang, W. Gong, S. Shi, L. Du, B. Zhu, J. Sun, and S. Song</i>	977
An Indoor Backpack System for 2-D and 3-D Mapping of Building Interiors	<i>C. Wen, S. Pan, C. Wang, and J. Li</i>	992

About the Cover: Mini-RF radar onboard the Lunar Reconnaissance Orbiter (LRO) mission was launched by NASA (October 2009) with a main objective to detect the presence of water ice in permanently shadowed regions (PSRs) over lunar poles. The spatial resolution of the Mini-RF dataset is 7.4 m/pixel, and in the figure, each pixel is coded with different color to indicate the different percentage of water ice within Hermite-A crater. The reddish color indicates low percentage of water ice, while bluish shade indicates higher percentage of water ice. It is observed from the analysis that about 66.32% of PSR area of Hermite-A is covered with different percentage of water ice ranging from 1% to 9%, while in the remaining 33.68% area does not have water ice. For more information please see “Quantification of Water Ice in the Hermite-A Crater of the Lunar North Pole” by Calla *et al.*, which begins on page 926.